J Musculoskelet Neuronal Interact 2014; 14(3):267-275

Original Article

Hylonome

Tibia segment deformation in response to simulated muscle forces: a cadaveric study with a novel optical segment tracking (OST) approach

P-F. Yang[1,2,3], K. Engel[3], M. Sanno[3], J. Dargel[4], K. Wegmann[4], G-P. Brüggemann[3], J. Rittweger[2]

[1]Key Laboratory for Space Bioscience and Biotechnology, School of Life Sciences, Northwestern Polytechnical University, Xi'an, China; [2]Institute of Aerospace Medicine, German Aerospace Center, Cologne, Germany; [3]Institute of Biomechanics and Orthopaedics, German Sport University Cologne, Cologne, Germany; [4]Department of Orthopaedic and Trauma Surgery, University of Cologne, Cologne, Germany

Abstract

Objectives: A novel optical segment tracking (OST) approach reliant upon motion capturing was previously proposed to assess human tibia segment deformation. The purposes of the present study were to validate the OST approach and assess the contribution of muscular forces to the bone deformation in a well-defined *ex vivo* human model. **Methods:** A custom-made Lower Extremity Loading Device (LELD) was developed to simulate physiological muscle contractions in six human cadaveric lower extremities. Tibia segment deformation was measured by tracking the relative movement between two marker clusters which were affixed into the proximal and distal tibia, respectively. **Results:** Compared to the physiological norms, the simulated muscle forces remained at a low level. When quadriceps muscle was loaded with forces from 198 N to 505 N, posterior bending (0.12°-0.25°) and lateral bending (0.06°-0.21°) of the tibia segment were found. Large tibia bending angles were found when simulating the co-contraction of upper leg muscles and plantar flexors, and of all leg muscles, respectively. The standard deviations of the deformation angles between the repetitions remained at a low level. **Conclusions:** We conclude that the OST approach has the potential to be applied *in vivo* and quantify muscle-induced bone deformations.

Keywords: Tibia Deformation, Bending and Torsion, Simulated Muscle Contractions, Optical Approach, *Ex Vivo*

Introduction

Numerous animal studies suggested that bone strain plays a crucial role in the mechano-adaption of bones[1,2]. However, our current understanding of such bone strains in humans is still limited due to technical difficulties. Bones of the lower extremity in humans bear body weight during bipedal locomotion. Meanwhile, the muscles provide the major driven forces to move the body forward. Close relationships between regional muscle and bone have been observed in many morphological[3] and functional studies[4,5]. For instance, forearm muscle cross-section area can be another surrogate, besides the grip torques, for estimating the radius bone strength in health older adults[6,7]. Evidence suggested that both body mass and muscle cross-section area contribute to the tibia bone content and estimated strength[7]. However, whether the muscle forces or gravitation-derived force predominates the mechanical loading of the bones in the lower extremities is still under debate[8,9]. To date, it has not been fully understood how muscle forces act on bone and contribute to bone loading.

As the most direct approach towards the mechanical loading on bone, the traditional strain gauge methods have been mostly relied on to assess the *in vivo* bone deformation in humans[10,11]. The intrinsic shortcomings of strain gauge methods, *e.g.* bonding-bending problems and less informative issues, have been recently discussed[12]. In order to overcome the drawbacks of the strain gauge methods, an optical segment tracking (OST) approach and its possible application in humans have been proposed for bone deformation measurements[13]. The concept of the OST approach is straightforward, namely to derive bone

The authors have no conflict of interest.

Corresponding author: Peng-Fei Yang, Key Laboratory for Space Bioscience and Biotechnology, School of Life Sciences, Northwestern Polytechnical University, Xi'an, China, Youyi Xilu 127, 707#, 710072, Xi'an, China
E-mail: yangpf@nwpu.edu.cn

Edited by: S. Warden
Accepted 24 July 2014

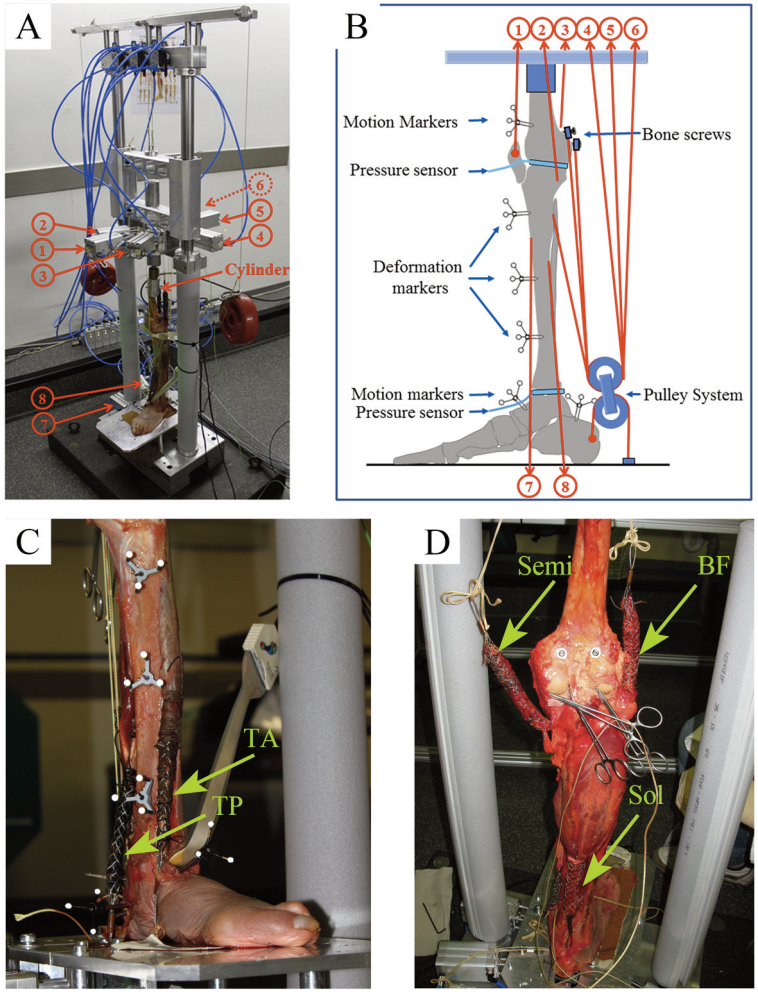

Figure 1. Illustrations of the LELD and loading configuration of the tibia. 1-8 refers to the different pneumatic actuators linked to different muscles. 1: quadriceps (Qua), 2: semimembranosus/tendinosus (Semi), 3: biceps femoris (BF), 4: gastrocnemius medialis (GM), 5: soleus (Sol), 6: gastrocnemius lateralis (GL), 7: tibialis anterior (TA), 8: tibialis posterior (TP). A: a cadaveric specimen was fixed on the LELD. B: the loading configuration and the pulley system. The red lines represent the muscles or connecting ropes. C: The muscle belly of TA and TP was enmeshed with wire network of the finger sleeves and connected to the pneumatic actuators from LELD through ropes. D: The muscle belly of Semi, BF and Sol was enmeshed with finger sleeves and connected to the pneumatic actuators from LELD through ropes.

deformation from the relative movement of marker clusters affixed to different locations of a given bone. Specifically, if few retro-reflective marker clusters with three non-collinear markers on each cluster are anchored into the anterior-medial aspect of tibia by bone screws, tibia deformation, *e.g.* bending angle and torsion angle, can be derived. Of note, a particular optimized configuration of the optical system has to be adopted to achieve sufficient recording resolution, accuracy and precision of the marker's movement in 3D volume.

However, the practical feasibility of the OST approach has not been assessed before. The purpose of the study presented in this paper was to further validate the OST approach for tibia deformation measurements in a cadaveric model. More specifically, the cadaveric tibia was loaded by simulated muscle forces with a custom-made Lower Extremity Loading Device (LELD). The influences of the simulated muscle forces on tibia deformations of the cadaveric tibia were thus investigated with the OST approach.

Materials and Methods

Lower Extremity Loading Device (LELD)

The Lower Extremity Loading Device (LELD, Figure 1A) was developed to fix the cadaveric specimens and apply the simulated muscle force to the cadaveric tibia by activating the pneumatic actuators. More specifically, the LELD consisted of two vertical steel beams, which were fixed on the base plate to support the upper aluminum plate. The lower aluminum plate was anchored with pneumatic actuators (Figure 1A). The height of the upper plate was adjustable and able to slide along

the vertical beams upward or downward to suit different specimens. One of the pneumatic actuators (ADN-50-60-I-P-A, theoretical force 1178 N at 6 bar, maximum pressure 10 bar, Festo, Esslingen, Germany) fixed on the upper plate was for connecting the patella and could simulate quadriceps (Qua) muscle contractions. Five other pneumatic actuators (ADN-40-60-I-P-A, theoretical force 754 N at 6 bar, maximum pressure 10 bar, Festo, Esslingen, Germany) were used to simulate the contractions of biceps femoris (BF), semimembranosus and semitendinosus in combination (Semi), gastrocnemius medialis (GM), gastrocnemius lateralis (GL), and soleus (Sol), respectively. On the bottom aluminum plate of the LELD, two more pneumatic actuators (ADN-40-60-I-P-A, theoretical force 754 N at 6 bar, maximum pressure 10 bar, Festo, Esslingen, Germany) were used to simulate tibialis anterior (TA) and tibialis posterior (TP) muscle contractions, respectively. The ropes between the finger sleeves and the actuators allowed the stretch force transmission to individual muscle to simulate physiological muscle forces.

In general, the gastrocnemius muscles and Sol muscle together contribute forces to the Achilles tendon, through calcaneus and the ankle joint, and finally to the distal tibia. On the other side, an opposing force with equal amplitude was applied onto the distal femur and proximal tibia through the origins of these two muscles. Considering this fact, and in order to simulate the mechanical loading on the tibia as close to physiological conditions as possible, a custom-made pulley system (Figure 1B) was invented. Ropes from gastrocnemius and Sol muscles were looped over the pulley which was affixed to the calcaneus, redirected and connected to the upper pneumatic actuators to allow the application of forces on the gastrocnemius muscle, Sol muscle and calcaneus simultaneously (Figure 1B).

The dissected femora of the specimens were mounted in an aluminum cylinder, which was a part of the upper aluminum plate (Figure 1A), with polymethyl methacrylate and centered in the mounting cylinder by centering screws. Prior to the measurements, neutral vertical position (0° knee joint and 90° ankle joint) of the leg was defined by adjusting the femur-mounting cylinder and ensured the plantar surface of the foot on the bottom aluminum plate. The long axis of the leg was oriented visually to be vertically aligned by an experienced clinician.

Cadaveric specimens

Six fresh frozen human cadaveric lower extremities, including the intact lower leg and truncated thigh, were used in this study. They were from three donors, namely a 67 year-old man, a 92 year-old woman and a 94 year-old woman. The specimens were obtained by transection at the thigh approximately 20 cm above the knee joint. The knee joint, tibia, ankle joint and the foot were kept intact. The specimens were defrosted over 24 hours prior to the measurements.

The specimens were prepared by carefully removing the soft tissue above the malleolus and separating the following muscles or muscle groups, including Qua, BF, Semi, GM, GL, Sol, TA and TP. The Qua muscle was dissected from the distal tendon and detached from the patella. A rope linked to one of the pneumatic actuators from LELD was connected with patella by custom-made connector to allow the application of simulated muscle force. The proximal tendon of TA, TP (Figure 1C), BF and Semi (Figure 1D) and the distal tendon of Sol (Figure 1D) were cut and enmeshed, respectively, with the steel wire network of the finger sleeves (Dr. Paul Koch GmbH, Frickenhausen, Germany, Figure 1C and Figure 1D) which normally are used in the hand traction system during wrist and hand surgery to position the hand. These finger sleeves were connected to the pneumatic actuators in the LELD to allow the application of the simulated muscle forces. Since the insertions of the GM and GL on femur are much localized and it was difficult to fully separate these two muscles, the GM and GL were dissected from the proximal tendon. Instead of their tendon insertion into the femur, two bone screws (Ø4.5 mm, 30 mm length, Marquardt Medizintechnik GmbH, Germany) were inserted into the proximal insertions in femur and connected to the pneumatic actuators from LELD with ropes to allow the application of the simulated muscle forces.

The muscle loading protocol

The output stretching forces of pneumatic actuators were controlled manually by adjusting a knob and also automatically by a custom-programmed Labview routine (v. 2009, National Instrument, TX, USA).

Prior to running the loading protocol, the possible maximum forces for different muscles were assessed by manually controlling the individual pneumatic actuator and increasing the load on muscles until a visible stretching was identified. The stretching of the muscles mostly relies on the experience of the research staff. The manual loading procedure was immediately stopped once there were slight trend of muscle rupture, *i.e.* excessive sliding between the muscle tissue, during the loading procedure. The force at that time was thus taken as the maximum loading force of the tested muscle. It was thus possible to calculate the expected applied muscle forces in the loading protocol according to the ratio of muscles' physiological cross section area[14,15]. For the upper leg, Semi and BF were always loaded and released simultaneously and their forces were set at 30% of Qua muscle force[14,15]. For the lower leg, the maximum forces of TP and TA were set at 25%, 10% of triceps surae muscle force, respectively. The maximum forces of GM and GL were set at 35% and 15% of the Sol muscle force[16]. Each muscle was preloaded with 20 N prior to all loading protocols to maintain a tight actuator-muscle connection.

The loading patterns are summarized in Table 1. Three groups of muscle loading patterns were included in the present study: 1) The loading patterns to simulate 7 individual muscle contractions; 2) The loading patterns to simulate the muscle co-contractions; 3) The loading patterns to simulate the muscle activities during the stance phase of a gait cycle, including from heel contact to opposite toe-off (G1, 0-10% of the gait cycle), from opposite toe-off to neutral body position (G2, 10-20% of the gait cycle), from neutral body position to opposite heel contact (G3, 30-50% of the gait cycle) and from opposite heel contact to toe-off (G4, 50-60% of the gait cycle), respectively. Under each load-

		Qua	Hamst	Sol	GM	GL	TA	TP
Individual muscle	Qua	×						
	Hamst		×					
	Sol			×				
	GM				×			
	GL					×		
	TA						×	
	TP							×
Co-contraction	P1				×	×		
	P2			×	×	×		
	P3			×	×	×	×	×
	P4	×	×	×	×	×		×
Simulated gait	G1	×	×	×	×	×	×	
	G2	×	×	×	×	×	×	×
	G3			×	×	×		×
	G4					×	×	

'×' indicated that the muscles were active. Qua: Quadricpes muscle, Hamst: hamstrings, namely biceps femoris (BF) and semimembranosus/tendinosus, Sol: soleus muscle, GM: gastrocnemius medialis muscle, GL: gastrocnemius lateralis muscle, TA: tibialis anterior muscle, TP: tibialis posterior muscle. P1, P2, P3 and P4 referred to the loading patterns in which muscle co-contractions were simulated. G1, G2, G3 and G4 referred to the muscle activities during 0-10%, 10-20%, 30-50% and 50-60% of a gait cycle (stance phase), respectively.

Table 1. The loading protocol of the muscles or muscle groups.

ing condition, tibia deformations were recorded when the muscles were loaded from baseline, *i.e.* 20 N, increasing until reaching the plateau, *i.e.* the maximum force, for 5 seconds.

Optical segment tracking for tibia deformation recording

The motion capturing OST approach has been described in detail elsewhere[13]. Briefly, three deformation marker clusters with three non-collinear retro-reflective markers (Ø5 mm, Géodésie Maintenance Services, Nort Sur Erdre, France) on each cluster were affixed into the antero-medial aspect of tibia cortex by bone screws (Cannulated screws, Ø3 mm, 24/6 mm, Stryker Leibinger GmbH & Co. KG, Germany). The sites for inserting bone screws were approximately 10 cm below the tibia plateau, mid-site of the tibia diaphysis and approximately 10 cm above the tibia medial malleolus, respectively. The bone screws were inserted into tibia visually perpendicular to the bone surface and penetrated into tibia approximately 3 mm to remain the bone screws in the cortical tibia.

Using the Vicon MX motion capture system with five Vicon F40 cameras (Vicon Motion System Ltd., CA, USA), the trajectories of the retro-reflective markers were captured during the above-mentioned loading protocols. The umbrella distribution of the cameras, manual calibration, close camera distance (<90 cm), and small markers were used according to our previous recommendations[13].

Determination of the Shank Anatomical Coordinate System (SACS)

The coordinates of the anatomical landmarks of the shank within the global coordinate system were positioned by a marker pointer prior to the tibia deformation measurements. The marker pointer consisted of three non-collinear markers and a pin (Figure 2). The coordinates of these three markers were recorded when the tip of the pin pointed against the distal apex of the lateral, medial malleolus, the prominence of the tibial tuberosity and the head of fibula, respectively. Since the relative position between three non-collinear markers and the tip of the pin was known and constant, it was therefore possible

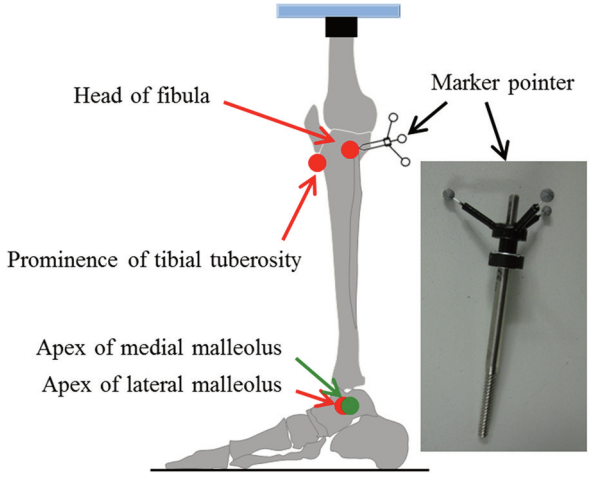

Figure 2. The determination of the Shank Anatomical Coordinate System (SACS). Red and green spots referred to the anatomical landmarks. The tip of the marker pointer pointed against these landmarks during the coordinate recording.

	Achieved maximum force level (N)						
Specimens	**Qua**	**Hamst**	**Sol**	**GM**	**GL**	**TA**	**TP**
A	505	152	308	108	46	46	116
B	340	102	214	75	32	32	80
C	198	59	164	58	24	24	62
D	491	147	307	107	46	46	115
E	439	132	174	60	26	26	65
F	248	74	137	48	21	21	51

Qua: Quadricpes muscle, Hamst: hamstrings, namely biceps femoris (BF) and semimembranosus/tendinosus, Sol: soleus muscle, GM: gastrocnemius medialis muscle, GL: gastrocnemius lateralis muscle, TA: tibialis anterior muscle, TP: tibialis posterior muscle.

Table 2. The force level for different muscles during the loading protocol.

to calculate the coordinates of the anatomical landmarks, from which the SACS was thus determined[17]. The trajectories of all markers for tibia deformation and determination of the SACS were captured at 200 Hz.

Data analysis

Marker trajectories of the proximal and distal marker clusters over 2 seconds after the simulated muscle forces reaching the plateau were used to compute the tibia deformation. A custom-written Matlab routine (The MathWorks, Inc. Version 7.9.0 R2009b) processed the raw trajectory data of all markers.

Tibia deformation was computed from the relative movement of the proximal and distal tibia-affixed markers, representing as the antero-posterior, medio-lateral bending angle and internal-external torsion angle of proximal tibia with respect to the distal tibia. Briefly, the coordinates of tibia-affixed markers in SACS were determined firstly by coordinate transformation[18,19]. The relative movement between the proximal and distal marker clusters was then computed and expressed as the relative movement in 6 degrees of freedom in the SACS, *i.e.* three Cardan/Euler rotation angles and three translations along the different axis of the SACS. The most representative results, *i.e.* bending and torsion angles, were reported as of tibia deformation. Each loading protocol was repeated three times to assess the repeatability of the measurements. In order to assess how widely scattered the repeated measurements were, *i.e.* whether the tibia deformation can really be repeatable with the OST approach, results were presented as mean and standard deviation (mean ± S.D.). The tibia deformation angles were plotted using Graphpad Prism statistical software (version 5.00, GraphPad software, Inc., La Jolla, CA).

Results

Muscle forces

Compared to normal physiological situations, the forces achievable with the cadaveric muscles were rather low. The maximum muscle forces we were capable to apply ranged from 68 N to 505 N for all the muscles/tendons in all of the specimens. The muscle forces were maintained in a low level to avoid the tendon/muscle rupture. The achieved maximum muscle forces were summarized in Table 2. For some specimens, muscles were ruptured after few times of repeated stretching. The corresponding data was thus discarded.

Tibia deformation under the relatively large muscle forces: When loading the quadriceps muscle with forces ranging between 198 N to 505 N, the proximal tibia compressed towards the lateral aspect by 0.06°±0.01° to 0.21°±0.04° in five specimens (Table 3), and bending also occurred towards the posterior aspect with respect to the distal tibia by 0.12°±0.01° to 0.25°±0.00° for all specimens (Table 3). Tibia deformation in five specimens, except specimen C, followed the same pattern across different loading conditions. Besides, relatively large tibia bending angles were measured in 'P4', 'G1' and 'G2' loading protocols as well. The amplitude ranged between 0.09°±0.00° and 0.26°±0.01° for the lateral bending (Table 4) and from 0.01°±0.00° to 0.17°±0.01° for the posterior bending (Table 4), respectively.

Anterior bending angles: In contrast to the posterior bending detected under the other loading conditions, anterior bending angles were measured from 0.03±0.00° to 0.10±0.00° when hamstrings, namely BF and Semi, were loaded (Table 3).

Torsion angles: Compared to the lateral and posterior bending angle, the torsion angle was relatively small. However, a similar torsion pattern can still be observed with different loading patterns. For instance, external torsion of the proximal tibia was indicated in 4 of all specimens, ranging from 0.02±0.00° to 0.08±0.02° and from 0.04±0.02° to 0.11±0.00° when 'Sol' and 'P2' loading protocol was applied, respectively (Table 3 and Table 4).

Repeatability of the deformation recording: The variation between the repeated measurements remained at a very low level, which can be shown with the small standard deviation of the mean deformation angles for lateral bending angles, internal rotation angles and posterior bending angles, respectively (Table 3 and Table 4).

The tibia deformations, mainly the lateral bending angles, posterior bending angles and internal torsion angles of all specimens in all loading conditions were summarized in Table 3 and Table 4.

Specimen	Def. Regime	Tibia deformation angles (Degree) under different loading pattern						
		Qua	BF	GM	GL	Sol	TP	TA
A	Lat. Bending	0.11±0.00	-0.01±0.01	0.00±0.00	0.03±0.01	0.01±0.00	0.01±0.01	0.03±0.00
	Int. Torsion	0.01±0.01	0.00±0.01	0.01±0.00	0.00±0.00	0.00±0.02	0.02±0.00	0.00±0.01
	Pos. Bending	0.12±0.01	-0.05±0.01	0.01±0.00	0.01±0.01	0.01±0.00	-0.02±0.01	0.00±0.00
B	Lat. Bending	0.10±0.00	-0.01±0.00	0.00±0.00	0.01±0.01	-0.02±0.01	N/A	0.02±0.01
	Int. Torsion	0.02±0.02	0.01±0.01	-0.04±0.00	0.01±0.01	-0.08±0.02	N/A	0.01±0.01
	Pos. Bending	0.23±0.00	-0.06±0.02	-0.02±0.00	0.00±0.00	-0.01±0.02	N/A	0.01±0.01
C	Lat. Bending	-0.04±0.03	0.02 ± 0.00	0.01±0.01	0.00±0.01	0.02±0.01	0.00±0.02	0.00±0.01
	Int. Torsion	0.09±0.01	0.01 ± 0.04	-0.01±0.01	0.00±0.01	-0.02±0.00	-0.01±0.00	0.00±0.01
	Pos. Bending	0.11±0.03	-0.05 ± 0.03	0.02±0.01	0.00±0.00	-0.03±0.01	-0.01±0.00	0.00±0.01
D	Lat. Bending	0.21±0.04	-0.02±0.02	0.00±0.01	0.02±0.00	-0.01±0.00	-0.01±0.01	0.03±0.02
	Int. Torsion	0.08±0.01	0.05±0.01	0.03±0.01	0.01±0.00	-0.03±0.03	0.02±0.01	0.02±0.01
	Pos. Bending	0.11±0.01	-0.03±0.00	0.01±0.01	0.00±0.00	-0.01±0.00	-0.01±0.01	-0.03±0.02
E	Lat. Bending	0.06±0.01	-0.05±0.00	0.00±0.00	0.00±0.01	N/A	0.02±0.00	0.00±0.00
	Int. Torsion	0.04±0.02	-0.03±0.00	0.00±0.01	0.01±0.00	N/A	0.02±0.02	0.00±0.00
	Pos. Bending	0.25±0.00	-0.10±0.00	0.00±0.01	0.00±0.00	N/A	0.01±0.01	0.00±0.00
F	Lat. Bending	0.07±0.00	-0.02±0.00	0.01±0.01	N/A	0.09±0.00	0.09±0.00	0.17±0.00
	Int. Torsion	0.07±0.02	-0.03±0.01	-0.01±0.01	N/A	-0.07±0.00	0.01±0.01	0.00±0.01
	Pos. Bending	0.17±0.01	-0.05±0.00	0.00±0.01	N/A	0.04±0.00	0.01±0.00	-0.02±0.00

Def.: the abbreviation of 'deformation'. Lat. Bending, Int. Torsion and Pos. Bending referred to lateral bending, internal torsion and posterior bending of the proximal tibia. Negative mean value indicated the medial bending, external torsion and anterior bending of the proximal tibia. Qua: Quadricpes muscle, Hamst: hamstrings, BF: biceps femoris, Semi: semimembranosus/tendinosus, Sol: soleus muscle, GM: gastrocnemius medialis muscle, GL: gastrocnemius lateralis muscle, TA: tibialis anterior muscle, TP: tibialis posterior muscle. N/A: deformation data was not available due to the muscle rupture prior to the loading experiments.

Table 3. Tibia deformation angles under simulated muscle force of individual muscle.

Specimen	Def. Regime	Tibia deformation angles (Degree) under different loading pattern							
		P1	P2	P3	P4	G1	G2	G3	G4
A	Lat. Bending	0.02±0.01	0.04±0.01	0.09±0.03	0.25±0.01	0.25±0.01	0.24±0.00	0.07±0.01	0.03±0.00
	Int. Torsion	-0.02±0.00	-0.04±0.02	-0.01±0.01	-0.02±0.01	0.03±0.03	0.02±0.01	0.00±0.02	0.02±0.01
	Pos. Bending	0.03±0.00	0.01±0.00	0.02±0.00	0.11±0.00	0.13±0.00	0.10±0.01	0.02±0.00	-0.01±0.00
B	Lat. Bending	0.00±0.01	-0.00±0.01	0.01±0.00	0.09±0.00	0.09±0.00	N/A	N/A	N/A
	Int. Torsion	0.01±0.01	-0.11±0.00	-0.09±0.00	0.01±0.00	0.00±0.01	N/A	N/A	N/A
	Pos. Bending	0.00±0.00	-0.04±0.01	-0.03±0.00	0.17±0.01	0.17±0.00	N/A	N/A	N/A
C	Lat. Bending	0.01±0.01	0.01±0.00	0.00±0.01	-0.08±0.00	-0.09±0.01	-0.07±0.00	0.03±0.01	0.00±0.00
	Int. Torsion	0.02±0.00	0.03±0.02	0.01±0.04	0.04±0.00	0.08±0.01	0.07±0.00	0.02±0.01	0.01±0.01
	Pos. Bending	0.11±0.03	-0.05±0.03	0.02±0.01	0.00±0.00	-0.03±0.01	-0.01±0.00	N/A	0.00±0.01
D	Lat. Bending	-0.02±0.01	-0.01±0.01	0.00±0.00	0.22±0.00	0.25±0.02	0.26 ± 0.01	0.06±0.01	-0.01±0.00
	Int. Torsion	-0.03±0.01	0.00±0.00	-0.02±0.01	0.05±0.03	0.07±0.02	0.09 ± 0.01	-0.08±0.01	-0.03±0.00
	Pos. Bending	-0.01±0.02	0.02±0.01	-0.02±0.01	0.02±0.03	0.03±0.00	0.01 ± 0.00	-0.06±0.00	-0.01±0.00
E	Lat. Bending	N/A	N/A	N/A	N/A	N/A	N/A	N/A	0.00±0.00
	Int. Torsion	N/A	N/A	N/A	N/A	N/A	N/A	N/A	0.00±0.00
	Pos. Bending	N/A	N/A	N/A	N/A	N/A	N/A	N/A	0.00±0.00
F	Lat. Bending	-0.01±0.00	0.07±0.01	0.07±0.00	0.11 ± 0.00	0.11 ± 0.00	0.11±0.01	N/A	N/A
	Int. Torsion	-0.01±0.01	-0.11±0.00	-0.10±0.00	-0.01 ± 0.01	0.02 ± 0.01	N/A	N/A	N/A
	Pos. Bending	0.00±0.00	0.05±0.01	0.04±0.00	N/A	0.15 ± 0.00	0.16±0.00	N/A	N/A

Def.: the abbreviation of 'deformation'. Lat. Bending, Int. Torsion and Pos. Bending referred to lateral bending, internal torsion and posterior bending of the proximal tibia. Negative mean value indicated the medial bending, external torsion and anterior bending of the proximal tibia. P1, P2, P3 and P4 referred to the loading pattern in which muscle co-contractions were simulated. G1, G2, G3 and G4 referred to the muscle activities during 0-10%, 10-20%, 30-50% and 50-60% of gait cycle (stance phase), respectively. N/A: deformation data was not available due to the muscle rupture prior to the loading experiments.

Table 4. Tibia deformation angles under simulated muscle force of individual muscle.

Discussion

The presented study assessed tibia deformation in a cadaveric model using a novel optical segment tracking (OST) approach. A simulation of the lower extremity musculature was achieved using a Lower Extremity Loading Device (LELD) on cadaveric specimens. Results suggest that tibia deformation angles could be assessed with the OST approach. The deformation angles varied under different loading protocols. Relatively large tibia deformation angles were observed when Qua muscle forces and the co-contraction of muscle groups were simulated, with the peak posterior bending angle up to 0.25º, and the peak lateral bending angle reaching up to 0.26º. Most importantly, the variation between the repeated measurements remained on a very low level, which was indicated with the small standard deviation value (Table 3 and Table 4). Therefore, it seems that the OST approach can assess whole-bone deformation with high accuracy and reproducibility.

Simulated muscle forces

Simulation of the physiological muscle forces *ex vivo* is a well-known difficulty in cadaveric studies. Given the tissue degradation *post mortem*, mostly by freezing, and the reduced mechanical properties of the tissue *ante mortem* based on the donor's age and medical record, the low levels of muscle simulation forces were no great surprise in this study. These forces are clearly not comparable to the *in vivo* situations, for instance, the soleus muscle force can reach up to ~2500 N *in vivo* during the maximum tetanic contractions[20]. Many studies used tendon as a mediator to transmit expectedly large force to the segment in the cadaver models, *e.g.* freeze clamping techniques[21,22], but this is impossible when dealing with muscle origins *e.g.* of the Sol muscle, as the proximal insertion of the Sol are too short for freeze clamping techniques. Loading Sol muscle downwards through the Achilles tendon using freeze clamping techniques may deliver relatively large force, but thus the equal force to the calcaneus can not be simulated. In the present model, the mechanical load on both proximal and distal tibia from the adjunct bones, ligaments and muscles were simulated. The loading regimes were therefore simulated as close as possible to the physiological condition. The muscle belly grasping technique with the finger sleeves in the presented study did show its ability of forces transmission. However, the limited ability of the cadaveric muscles to resist stretching forces generated by the pneumatic actuators attenuated the forces to much lower levels than *in vivo* physiological loads.

Furthermore, the fasica was believed to play an important role in the force transmission from the muscles to bone[23]. In the present study, the intact fascia was dissected in order to isolate different muscles, leading the releasing of the proximal or distal muscle belly from the tibia. It is therefore speculated that low simulated muscle force and the lack of force transmission by fasica to tibia might be the main reasons of tibia deformation angles being limited.

Muscle forces induced tibia deformation

Instructive results were achieved in relation to muscle-bone interaction effects. For most of the loading patterns, posterior bending of the tibia was observed. This was expected given the anatomical structure of the musculoskeletal system in human lower leg. The plantar flexors are located at the posterior aspect of the tibia. A considerable posterior moment, which induces the posterior bending of tibia, can be induced by the contraction of the plantar flexors. More interestingly, the present results provide detailed insight into the muscular contributions to the tibia mechanical loads and the musculoskeletal mechanics of the human lower limb. For instance, lateral (positive deformation value in Table 3) and posterior bending (positive deformation value in Table 3) of the proximal tibia primarily occurred while the quadriceps muscles were loaded. By contrast, the medial and anterior bending (negative deformation value in Table 3) were found when the hamstrings muscles were loaded. Moreover, tibia deformation amplitude varied greatly while the different muscle contractions were simulated. Of note, the lateral bending regime of the specimen C under P4, G1 and G2 loading situations were different with that of the other specimens (Table 4). The inconsistency of the tibia deformation angles across the specimens may be due to the placement of the specimen in the LELD prior to the loading experiments. As mentioned previously, the long axis of the leg was placed to the LELD by an experienced clinician. The slight positioning difference between the specimens could exist, which may thus yield different mechanical environment on tibia during simulated muscle contractions. More precisely controlling the loading environment of the tibia would be appreciated in future studies.

Potential applications of the OST approach

It has been well accepted that bone strain (or strain rate) level is a classical parameter to assess bone responses to mechanical stimuli. Our current knowledge of *in vivo* bone strain data is mostly obtained from the strain gauge approaches, which can generally provide local strain results at a specific site. However, strain is not uniformly distributed across the entire bone surface. The extremely complex *in vivo* bone strain may contain much information, which may have been disregarded or mis-interpreted in the previous 'strain-gauge' studies[24]. In the future studies, by integrating subject-specific bone modeling methods, *i.e.* finite element modeling of tibia, and the tibia segment deformation derived from the OST approach, local bone strain and strain distribution can thus be calculated, which may provide new knowledge on the *in vivo* tibia strain in humans if the OST approach can be applied in humans.

Compared to the local bone strain, the mechanical environment of bone segment produced by muscle contractions, reaction forces or passive stretching forces from ligaments did not attract much attention in the past. In particular, it has been long debated on how muscles mechanically link to their adjacent bones. The loading regimes on bone primarily produced by regional muscle contractions remain unclear. With the OST approach, the loading regimes of the entire bone segment are possible to be investigated during locomotive activities. Combining with the approaches of assessing muscle activities, the potential contributions of the muscle contraction on bone load-

ing can be addressed, which will greatly further our understanding on how muscles mechanically link to the bones.

Like all the current available *in situ* bone deformation measuring techniques, the sites or bones to apply the OST approach *in vivo* are limited due to the interference of the adjacent muscle or the other soft tissue. Therefore, it would be challenging to apply the OST approach on femur, as the adjacent muscles of the femur may interfere with the bone screws and lead the unrealistic bone deformation results. Furthermore, the potential uncontrollable pain of the adjacent muscles induced by the installation of the bone screws may become another obstacle for the application of the OST approach on femur. Nevertheless, ulna is another possible bone, besides tibia, to apply the OST approach in humans. Of note, future studies are still needed to explore how to expand the application of the OST approach in humans.

Practically, in future *in vivo* experiments, the recruited volunteers would need to be prescribed approximately 4 weeks of restricted high impact exercises, as suggested by the experienced surgeons involved in the present study, after the extraction of the bone screws. However, it will not appear to affect the scientific strength of the OST approach and its technical advantages. Firstly, the OST approach certainly results in less damage to the periosteum and skin than strain gauge approaches during the installation of the bone screws into the tibia. Secondly, more informative results, *e.g.* tibia bending and torsion deformation regimes, can be derived than from strain gauge approaches. Thirdly, the application of bone screws in the OST approach can avoid the de-bonding issue of gauges in the strain gauge approaches.

Limitations

In the present study, one of the major limitations was that both simulated muscle forces and mechanical properties of the tibia vary from specimen to specimen, thus inflating the inter-specimen variation in tibia deformation enormously. Because of this, the presented tibia deformation amplitude in this paper was interesting in qualitative terms, but failed to provide true quantitative estimates of the tibia deformation induced by muscular forces. Furthermore, the value of the tibia deformation angles mostly remained at a low level due to the limited simulated muscle forces. However, as addressed previously, the major objective of the present research project was to validate the OST approach. The validation procedure included two aspects, the capability of the optical system to accurately capture the minute displacement and the feasibility of applying the OST approach in humans. The former has been demonstrated previously[13]; the later was shown in the present paper. The standard deviation of the repeated tibia deformation measurements in the present paper showed good reproducibility of the OST approach. From this perspective, the well-repeated tibia deformation angles, even with relative low amplitude generated by limited simulated muscle forces, are still capable of showing us the application feasibility of the OST approach in human bones. In consideration of the previously present resolution, accuracy and precision of the OST approach[13], it is suggested that the OST approach has the capability of quantifying even minute deformations of the tibia, which has been the main objective of the present study. We therefore speculate that the OST method will also be able to quantify muscle-induced bone deformation *in vivo*.

To conclude, the results demonstrated that the pattern and magnitude of tibia deformation can be modulated by the contraction of simulated muscle forces.

Acknowledgements

We would like to thank Hans-Martin Küsel-Feldker and Thomas Förster in the Institute of Biomechanics and Orthopaedics, German Sport University Cologne for designing and manufacturing the Lower Extremity Loading Device (LELD) and marker clusters adopted in this study. Special thanks to Sufyan Ali for his great technical support in controlling the LELD during the simulation of muscle forces and during data collection. Peng-Fei Yang acknowledges his scholarship by the China Scholarship Council (CSC No.: 2009629013).

References

1. Frost HM. Skeletal structural adaptations to mechanical usage (SATMU): 2. Redefining Wolff's law: the remodeling problem. The Anatomical record 1990;226:414-22.
2. Frost HM. Skeletal structural adaptations to mechanical usage (SATMU): 1. Redefining Wolff's law: the bone modeling problem. The Anatomical record 1990;226:403-13.
3. Rittweger J, Beller G, Ehrig J, et al. Bone-muscle strength indices for the human lower leg. Bone 2000;27:319-26.
4. Manske SL, Boyd SK, Zernicke RF. Muscle and bone follow similar temporal patterns of recovery from muscle-induced disuse due to botulinum toxin injection. Bone 2010;46:24-31.
5. Rittweger J, Felsenberg D. Recovery of muscle atrophy and bone loss from 90 days bed rest: results from a one-year follow-up. Bone 2009;44:214-24.
6. Frank AW, Lorbergs AL, Chilibeck PD, Farthing JP, Kontulainen SA. Muscle cross sectional area and grip torque contraction types are similarly related to pQCT derived bone strength indices in the radii of older healthy adults. J Musculoskelet Neuronal Interact 2010;10:136-41.
7. Frank AW, Labas MC, Johnston JD, Kontulainen SA. Site-specific variance in radius and tibia bone strength as determined by muscle size and body mass. Physiotherapy Canada Physiotherapie Canada 2012;64:292-301.
8. Judex S, Carlson KJ. Is bone's response to mechanical signals dominated by gravitational loading? Med Sci Sport Exer 2009;41:2037-43.
9. Robling AG. Is bone's response to mechanical signals dominated by muscle forces? Med Sci Sport Exer 2009; 41:2044-9.
10. Burr DB, Milgrom C, Fyhrie D, et al. *In vivo* measurement of human tibial strains during vigorous activity. Bone 1996;18:405-10.
11. Milgrom C, Finestone A, Simkin A, et al. In-vivo strain

measurements to evaluate the strengthening potential of exercises on the tibial bone. J Bone Joint Surg Br 2000; 82:591-4.
12. Yang PF, Bruggemann GP, Rittweger J. What do we currently know from *in vivo* bone strain measurements in humans? J Musculoskelet Neuronal Interact 2011;11:8-20.
13. Yang PF, Sanno M, Bruggemann GP, Rittweger J. Evaluation of the performance of a motion capture system for small displacement recording and a discussion for its application potential in bone deformation *in vivo* measurements. Proc Inst Mech Eng H 2012;226:838-47.
14. Friederich JA, Brand RA. Muscle fiber architecture in the human lower limb. Journal of biomechanics 1990;23:91-5.
15. Wickiewicz TL, Roy RR, Powell PL, Edgerton VR. Muscle architecture of the human lower limb. Clinical orthopaedics and related research 1983:275-83.
16. Albracht K, Arampatzis A, Baltzopoulos V. Assessment of muscle volume and physiological cross-sectional area of the human triceps surae muscle *in vivo*. Journal of Biomechanics 2008;41:2211-8.
17. Grood ES, Suntay WJ. A Joint Coordinate System for the Clinical Description of 3-Dimensional Motions - Application to the Knee. J Biomech Eng-T Asme 1983; 105:136-44.
18. Lafortune MA, Cavanagh PR, Sommer HJ 3rd, Kalenak A. Three-dimensional kinematics of the human knee during walking. Journal of biomechanics 1992;25:347-57.
19. Söderkvist I, Wedin P-Å. Determining the movements of the skeleton using well-configured markers. Journal of biomechanics 1993;26:1473-7.
20. Maganaris CN, Baltzopoulos V, Ball D, Sargeant AJ. *In vivo* specific tension of human skeletal muscle. J Appl Physiol 2001;90:865-72.
21. Sharkey NA, Hamel AJ. A dynamic cadaver model of the stance phase of gait: performance characteristics and kinetic validation. Clin Biomech (Bristol, Avon) 1998; 13:420-33.
22. Wunschel M, Leichtle U, Obloh C, Wulker N, Muller O. The effect of different quadriceps loading patterns on tibiofemoral joint kinematics and patellofemoral contact pressure during simulated partial weight-bearing knee flexion. Knee Surg Sports Traumatol Arthrosc 2011; 19:1099-106.
23. Huijing PA, Baan GC. Myofascial force transmission: muscle relative position and length determine agonist and synergist muscle force. Journal of Applied Physiology 2003;94:1092-107.
24. Rubin CT, Seeherman H, Qin YX, Gross TS. The mechanical consequences of load bearing in the equine third metacarpal across speed and gait: the nonuniform distributions of normal strain, shear strain, and strain energy density. FASEB J 2013;27:1887-94.